

EM-WaveHoltz: A flexible frequency-domain method built from time-domain solvers

Zhichao Peng and Daniel Appelö

Abstract—A novel approach to computing time-harmonic solutions of Maxwell’s equations by time-domain simulations is presented. The method, EM-WaveHoltz, results in a positive definite system of equations which makes it amenable to iterative solution with the conjugate gradient method or with GMRES. Theoretical results guaranteeing the convergence of the method away from resonances are presented. Numerical examples illustrating the properties of EM-WaveHoltz are given.

Index Terms—Maxwell equations, iterative method, electromagnetic analysis, frequency-domain analysis, time-domain analysis, FDTD methods, discontinuous Galerkin time-domain (DGTD) methods, positive definite

TWO of the main challenges when solving the time-harmonic Maxwell equations at high frequencies are the indefinite nature of the Maxwell system and the high resolution requirement. Without proper preconditioners, iterative solvers such as GMRES and BICG may converge slowly. These challenges are similar to the ones for solving the Helmholtz equation at high frequencies. Recently, we introduced a scalable iterative method called WaveHoltz [1] for the Helmholtz equation. In this paper, we introduce the electromagnetic-WaveHoltz (EM-WaveHoltz) method, which can be seen as a generalization of the WaveHoltz method to the time-harmonic (or frequency-domain) Maxwell equations. The proposed EM-WaveHoltz method converts the frequency-domain problem to a fix point problem in the time-domain. The fixed point iteration is linear and can be rewritten as a linear system of equations with a system matrix that is positive definite and that can therefore be efficiently inverted using standard Krylov methods such as GMRES.

In the EM-WaveHoltz method, we convert the frequency-domain problem to a time-domain problem by evolving and filtering Maxwell’s equations with periodic forcing over one time period. When applied, this filter results in the time-domain solution converging to a fix point where the solution becomes equivalent to the solution of the frequency-domain problem. Salient features of the EM-WaveHoltz method are as follows.

- 1) The resulting linear system is always positive definite (sometimes symmetric).
- 2) The EM-WaveHoltz method can be driven by any scalable time-domain solver, for example the finite difference time-domain (FDTD) method [2] and discontinuous Galerkin time-domain method (DGTD) [3].

- 3) A unique feature of the EM-WaveHoltz method is that it is possible to obtain frequency-domain solutions for multiple frequencies at once but at the cost of a single solve.

We note that properties of our method are to some extent shared with the properties of the controllability method. In particular the controllability method finds the solution to the frequency-domain problem by using time-domain solvers like our approach. However, while our formulation relies on a fixed point iteration, the controllability method seeks to minimize the deviation from time-periodicity of the initial and final data of the time-domain simulation. The controllability method was first proposed for a time-harmonic wave scattering problem [4], and we refer readers to [5] for recent development. The controllability method is also generalized to the time-harmonic Maxwell equation in second order formulation [6] and the first order formulation [7], [8]. One main difference between our method and the controllability method is that the controllability method needs backward solves, while our method does not.

There are of course many other methods that have been designed for efficiently solving the frequency-domain Maxwell’s equations. For scattering and radiation problems in homogeneous media integral equation formulations are known to be highly efficient and yield fast algorithms [9], [10]. Domain decomposition methods (DDM) [11] have also achieved success for the time-harmonic electromagnetic problems [12], [13], [14], [15], [16]. The DDM method and the integral equation method have been combined in [17]. Recently, [18] extends the “shifted-Laplacian preconditioner” for the Helmholtz equation to the high frequency time-harmonic Maxwell equations and designs an optimal DDM method. Multigrid methods have also been considered for the time-harmonic Maxwell equations [19], [20]. A multigrid method for the high frequency time-harmonic Maxwell equations is designed in [21]. Sweeping preconditioners for time-harmonic Maxwell equations, which utilize the intrinsic structure of the Green’s function, have been developed for the Yee scheme [22] and the finite element method [23]. We finally note that it is also possible to directly use a time-domain solver in other ways to find the frequency domain solution. The most straightforward approach is to save the solution for some time T and then take a Fourier transform. The upside with this approach is that it produces an approximate result to the frequency domain problem for many frequencies at once. The drawbacks are that the solution is approximate with an accuracy that, in the case of a continuous wave sinusoidal source, scales as T^{-1} and that the need to save

Zhichao Peng is with the Department of Mathematics, Michigan State University, East Lansing, MI 48824.

Daniel Appelö is with the Department of Computational Mathematics, Science & Engineering and the Department of Mathematics, Michigan State University, East Lansing, MI 48824

Manuscript received January 13, 2022; revised January 13, 2022.

the solution makes this approach memory intensive. This slow convergence can be improved if modulated sources are used and the resulting method can be more efficient than a single frequency solver if the frequency response is desired over a broad spectrum of frequencies and the accuracy requirements are less stringent. For open problems it is possible to appeal to the limiting amplitude principle [24] and simply let a harmonically forced problem converge to the frequency domain problem by simulating long enough. The convergence of this approach is severely impacted when trapping geometry is present and the principle is not valid for closed domains. Also for Fourier transformed methods the required simulation time becomes prohibitive when closed domains with the quality factor $Q = \infty$ are considered.

The rest of this paper is organized as follows. In Section I, we present the EM-WaveHoltz formulation for the continuous equations and discuss the properties of the resulting linear system, the choice of the linear solver, and present how to obtain solutions for multiple frequencies in one solve. In Section II, to show the flexibility with respect to the choice of the time-domain solvers, we couple the EM-WaveHoltz method, first with the Yee scheme and then with the discontinuous Galerkin (DG) method. In Section III, the performance of the EM-WaveHoltz method is demonstrated through a series of numerical examples. A simple implementation of the method in 1D to aid the reader in understanding the details of the method can be found at <https://zhichaopengmath.github.io/code/>.

I. ELECTROMAGNETIC WAVEHOLTZ ITERATION FOR THE MAXWELL'S EQUATION

We consider the frequency-domain Maxwell's equation:

$$i\omega\epsilon\mathbf{E} = \nabla \times \mathbf{H} - \mathbf{J}, \quad (1a)$$

$$i\omega\mu\mathbf{H} = -\nabla \times \mathbf{E}, \quad (1b)$$

closed by boundary conditions corresponding to either a perfect electric conductor or to an unbounded domain. Here \mathbf{E} and \mathbf{H} are the complex valued electric and magnetic fields, ϵ, μ are real valued permittivity and permeability and \mathbf{J} is the real valued current source. Taking the real and imaginary parts we find

$$-\omega\Im\{\epsilon\mathbf{E}\} = \Re\{\nabla \times \mathbf{H}\} - \mathbf{J}, \quad (2a)$$

$$\omega\Re\{\epsilon\mathbf{E}\} = \Im\{\nabla \times \mathbf{H}\}, \quad (2b)$$

$$-\omega\Im\{\mu\mathbf{H}\} = -\Re\{\nabla \times \mathbf{E}\}, \quad (2c)$$

$$\omega\Re\{\mu\mathbf{H}\} = -\Im\{\nabla \times \mathbf{E}\}. \quad (2d)$$

We want to relate the fields \mathbf{E} and \mathbf{H} to real valued and $T = 2\pi/\omega$ -periodic fields

$$\tilde{\mathbf{E}} = \hat{\mathbf{E}}_0 \cos(\omega t) + \hat{\mathbf{E}}_1 \sin(\omega t), \quad (3a)$$

$$\tilde{\mathbf{H}} = \hat{\mathbf{H}}_0 \cos(\omega t) + \hat{\mathbf{H}}_1 \sin(\omega t), \quad (3b)$$

that are solutions of the time-domain equations

$$\epsilon\partial_t\tilde{\mathbf{E}} = \nabla \times \tilde{\mathbf{H}} - \sin(\omega t)\mathbf{J}, \quad (4a)$$

$$\mu\partial_t\tilde{\mathbf{H}} = -\nabla \times \tilde{\mathbf{E}}. \quad (4b)$$

For such periodic solutions we can match the $\sin(\omega t)$ and $\cos(\omega t)$ terms to find the relations

$$-\omega(\epsilon\hat{\mathbf{E}}_0) = \nabla \times \hat{\mathbf{H}}_1 - \mathbf{J}, \quad (5a)$$

$$\omega(\epsilon\hat{\mathbf{E}}_1) = \nabla \times \hat{\mathbf{H}}_0, \quad (5b)$$

$$-\omega(\mu\hat{\mathbf{H}}_0) = -\nabla \times \hat{\mathbf{E}}_1, \quad (5c)$$

$$\omega(\mu\hat{\mathbf{H}}_1) = -\nabla \times \hat{\mathbf{E}}_0. \quad (5d)$$

Comparing (2a) with (5a) and (2c) with (5c), it now follows that the initial data of $\tilde{\mathbf{E}}$ and $\tilde{\mathbf{H}}$ matches the imaginary part of the frequency-domain solution

$$\Im\{\mathbf{E}\} = \hat{\mathbf{E}}_0, \quad \Im\{\mathbf{H}\} = \hat{\mathbf{H}}_0.$$

Also, from (2b), (5b) and (2d), (5d), we get

$$\Re\{\mathbf{E}\} = \hat{\mathbf{E}}_1 = \frac{1}{\epsilon}\nabla \times \hat{\mathbf{H}}_0, \quad \Re\{\mathbf{H}\} = \hat{\mathbf{H}}_1 = -\frac{1}{\mu}\nabla \times \hat{\mathbf{E}}_0. \quad (6)$$

Our EM-WaveHoltz method finds the periodic solutions (3) by iteratively determining the initial data to (4).

Define the filtering operator, Π , acting on the initial conditions $\boldsymbol{\nu} = (\boldsymbol{\nu}_E, \boldsymbol{\nu}_H)^T$:

$$\Pi\boldsymbol{\nu} = \Pi \begin{pmatrix} \boldsymbol{\nu}_E \\ \boldsymbol{\nu}_H \end{pmatrix} = \frac{2}{T} \int_0^T \left(\cos(\omega t) - \frac{1}{4} \right) \begin{pmatrix} \tilde{\mathbf{E}}_{\boldsymbol{\nu}} \\ \tilde{\mathbf{H}}_{\boldsymbol{\nu}} \end{pmatrix} dt, \quad (7)$$

with $T = 2\pi/\omega$ and $\tilde{\mathbf{E}}_{\boldsymbol{\nu}}$ and $\tilde{\mathbf{H}}_{\boldsymbol{\nu}}$ being the fields resulting from the initial conditions $\boldsymbol{\nu} = (\boldsymbol{\nu}_E, \boldsymbol{\nu}_H)^T$.

By construction $\Pi(\Im\{\mathbf{E}\}, \Im\{\mathbf{H}\})^T = (\Im\{\mathbf{E}\}, \Im\{\mathbf{H}\})^T$, and as $(\Re\{\mathbf{E}\}, \Re\{\mathbf{H}\})^T$ can be computed directly via (6), the solution to the frequency-domain equation is the fix-point of the operator Π .

The operator Π is contractive. Precisely, if a certain initial data gives rise to a solution that, in addition to the $\sin(\omega t)$ and $\cos(\omega t)$ terms in (3), has other time-harmonic components, e.g. $\sin(\omega' t)$, $\omega' \neq \omega$, then in each iteration the filter reduces the amplitude of those components.

Based on these facts, we define the EM-WaveHoltz iteration:

$$\boldsymbol{\nu}^{n+1} = \Pi\boldsymbol{\nu}^n, \quad \text{with } \boldsymbol{\nu}^0 = (\boldsymbol{\nu}_E^0, \boldsymbol{\nu}_H^0)^T = \mathbf{0}. \quad (8)$$

The EM-WaveHoltz iteration converges to the imaginary parts of the solution to the frequency-domain equation

$$\lim_{n \rightarrow \infty} \boldsymbol{\nu}^n = \lim_{n \rightarrow \infty} (\boldsymbol{\nu}_E^n, \boldsymbol{\nu}_H^n)^T = (\Im\{\mathbf{E}\}, \Im\{\mathbf{H}\})^T, \quad (9)$$

and the real parts can be recovered via (6).

Remark 1. Alternatively we could formulate the time-domain problem with a cosine forcing

$$\epsilon\partial_t\tilde{\mathbf{E}} = \nabla \times \tilde{\mathbf{H}} - \cos(\omega t)\mathbf{J}, \quad (10a)$$

$$\mu\partial_t\tilde{\mathbf{H}} = -\nabla \times \tilde{\mathbf{E}}. \quad (10b)$$

Again, the real valued $T = 2\pi/\omega$ -periodic solutions to (10) are of the form (3) but (see Appendix A) the solution to (10) $\tilde{\mathbf{E}}$ and $\tilde{\mathbf{H}}$ have a slightly different relation to the frequency-domain solution

$$\Re\{E\} = \hat{E}_0, \quad \Re\{H\} = \hat{H}_0, \quad \Im\{E\} = -\hat{E}_1, \quad \Im\{H\} = -\hat{H}_1.$$

With the same filter and iteration process defined as the sin-forcing case, we have

$$\lim_{n \rightarrow \infty} \boldsymbol{\nu}^n = \lim_{n \rightarrow \infty} (\boldsymbol{\nu}_E^n, \boldsymbol{\nu}_H^n)^T = (\Re\{\mathbf{E}\}, \Re\{\mathbf{H}\})^T. \quad (11)$$

In our numerical tests, we find that the number of iterations needed by the EM-WaveHoltz method are essentially identical for the two alternatives. In this paper, we focus on the EM-WaveHoltz with the sin-forcing.

A. EM-WaveHoltz for the energy conserving case

For real-valued ϵ , μ and J , with PEC boundary conditions and other boundary conditions that lead to a conservation of the electromagnetic energy in a bounded domain, the EM-WaveHoltz iteration can be simplified further. For such problems, assuming that ω is not a resonance frequency of the cavity, $\Im\{\mathbf{H}\}$ is identically zero and the EM-WaveHoltz iteration is reduced to

$$\boldsymbol{\nu}_E^{n+1} = \Pi \boldsymbol{\nu}_E^n, \quad \boldsymbol{\nu}_H^n = \mathbf{0}, \quad \boldsymbol{\nu}_E^0 = \mathbf{0}, \quad (12)$$

where now

$$\Pi \boldsymbol{\nu}_E = \frac{2}{T} \int_0^T \left(\cos(\omega t) - \frac{1}{4} \right) \tilde{\mathbf{E}}_{\boldsymbol{\nu}} dt. \quad (13)$$

As long as ω is not a resonance this simplified EM-WaveHoltz iteration converges

$$\boldsymbol{\nu}_E^n = \Im\{\mathbf{E}\}, \text{ as } n \rightarrow \infty. \quad (14)$$

B. Krylov acceleration

For unbounded problems where ω is close to a resonance or for bounded problems with trapping geometries, the convergence of the WaveHoltz fix point iteration can be slow [1]. Fortunately as the iteration is linear, it is easy to rewrite it as a positive definite linear operator that can be efficiently inverted by a Krylov subspace method. To see this we introduce the operator:

$$S\boldsymbol{\nu} = \Pi\boldsymbol{\nu} - \Pi\mathbf{0}. \quad (15)$$

Then, based on the definition of S , we have

$$\Pi\boldsymbol{\nu} = S\boldsymbol{\nu} + \Pi\mathbf{0}. \quad (16)$$

Hence, finding the fix point of Π : $\Pi\boldsymbol{\nu} = \boldsymbol{\nu}$ is equivalent to solving the equation $(I - S)\boldsymbol{\nu} = \Pi\mathbf{0}$. Here, we want to emphasize that $\Pi\mathbf{0} \neq \mathbf{0}$ unless frequency-domain problem has zero solutions (see (55) in Appendix B for more details). Here $\mathbf{0}$ stands for the zero initial condition in the time-domain, and with a non-zero source, the filtered time-domain solution over one period $\Pi\mathbf{0}$ is very likely nonzero.

A Krylov method such as the conjugate gradient method, GMRES or TFQMR can be applied to solve $(I - S)\boldsymbol{\nu} = \Pi\mathbf{0}$ in a matrix-free manner. In practice, to obtain the right hand side $\Pi\mathbf{0}$, we just need to solve the time-domain problem (4) with zero initial conditions $\boldsymbol{\nu} = \mathbf{0}$ from $t = 0$ to $t = T$ and use a numerical quadrature to approximate the filter $\Pi\mathbf{0}$ as we

march in time. To calculate the matrix multiplication $(I - S)\boldsymbol{\nu}$, we can utilize the fact that

$$(I - S)\boldsymbol{\nu} = \boldsymbol{\nu} - (\Pi\boldsymbol{\nu} - \Pi\mathbf{0}) = \boldsymbol{\nu} - \Pi\boldsymbol{\nu} + \Pi\mathbf{0}.$$

That is, for a given $\boldsymbol{\nu}$ and $\Pi\mathbf{0}$ precomputed, we just need to compute $\Pi\boldsymbol{\nu}$ to obtain the action of $(I - S)$ onto $\boldsymbol{\nu}$. Recall that $\Pi\boldsymbol{\nu}$ is obtained by computing the filter by a numerical quadrature incrementally as the solution to (4) is evolved for one $T = 2\pi/\omega$ period with $\boldsymbol{\nu}$ as the initial conditions. Thus the cost to compute one Krylov vector is that of a wave solve with one additional variable needed to sum up the projection throughout the evolution.

When using GMRES there is always a concern about the size of the Krylov subspace as the number of iterations grow. Here our method has a significant upside to solving the frequency-domain problem. Note that although we are looking for a $T = \frac{2\pi}{\omega}$ -periodic solution, there is nothing in the method that prevents us from changing the filtering to extend over a longer time, say, $T = N\frac{2\pi}{\omega}$, with N a positive integer. As we show in the numerical examples below, for moderate N this reduces the number of iterations by a factor of N so that the overall computational cost is the same. For GMRES without restart, filtering over longer periods reduces the memory needed. For GMRES with restart, filtering over longer periods reduces the number of restart needed.

In Appendix B, we show that $I - S$ is always a positive definite operator and for energy conserving boundary conditions it is also self-adjoint. These results carry over to the discretized equations in the sense that the matrix that needs to be inverted is always positive definite and, if a symmetric and energy conserving method (like the Yee scheme) is used, the matrix is also symmetric for energy conserving boundary conditions like PEC. For the SPD case our method becomes particularly efficient and memory lean as the conjugate gradient method can be used.

Now, we summarize how to implement the EM-WaveHoltz method given a time-domain solver and a GMRES iterative solver. The filtering is presented as Algorithm 1 and Algorithm 2 describes the GMRES/Krylov acceleration.

Algorithm 1: Given initial data $\boldsymbol{\nu}$ and a time-domain solver, compute $\Pi\boldsymbol{\nu}$.

- 1: Set $\boldsymbol{\nu} = (\boldsymbol{\nu}_E^T, \boldsymbol{\nu}_H^T)$ as the initial condition for the time-domain solver.
 - 2: Use the time domain solver to evolve the time-domain equation (10) for one/multiple periods. In each time step, incrementally compute $\Pi_h\boldsymbol{\nu}$ by the trapezoid rule for numerical integration.
 - 3: After the solution has been evolved for one period in time return $\Pi_h\boldsymbol{\nu}$.
-

C. Multiple frequencies in one solve

Similar to the WaveHoltz method for the Helmholtz equation [1], the EM-WaveHoltz method can be applied to obtain the solutions for multiple frequencies in one solve.

Algorithm 2: GMRES accelerated EM-WaveHoltz iteration.

- 1: Compute $\Pi\mathbf{0}$ by Algorithm 1.
 - 2: **procedure** MATMUL(ν) ▷ Compute $(I - S)\nu$.
 - 3: Use Algorithm 1 to compute $\Pi\nu$.
 - 4: **return** $(I - S)\nu = \nu - \Pi\nu + \Pi\mathbf{0}$.
 - 5: **end procedure**
 - 6: **procedure** SOLVE(TOL) ▷ Solve $(I - S)\nu = \Pi\mathbf{0}$
 - 7: Set the initial guess as $\nu^0 = (\mathbf{0}, \mathbf{0})^T$.
 - 8: Apply GMRES with matrix free MATMUL procedure. Stop if the relative residual is smaller than TOL.
 - 9: **end procedure**
 - 10: The solution produced by SOLVE is the imaginary part of the frequency-domain solution.
-

Precisely, let $\omega_k = n_k\omega_0$, $k = 1, \dots, N$ for some $\omega_0 > 0$ and $n_1 < n_2 < \dots < n_N$ being positive integers. Then in a traditional frequency-domain solver each frequency requires the solution of N different systems

$$i\omega_k \epsilon \mathbf{E}_k = \nabla \times \mathbf{H}_k - \mathbf{J}_k, \quad (17a)$$

$$i\omega_k \mu \mathbf{H}_k = -\nabla \times \mathbf{E}_k. \quad (17b)$$

Now, assuming that each frequency solve has the same type of boundary condition and material properties (the forcing \mathbf{J}_k can be different for each k), we can solve for all frequencies at once. We take the energy conserving case as an example, then the **single** time-domain problem we must solve is

$$\epsilon \partial_t \tilde{\mathbf{E}} = \nabla \times \tilde{\mathbf{H}} - \sum_{k=1}^N \sin(\omega_k t) \mathbf{J}_k, \quad (18a)$$

$$\mu \partial_t \tilde{\mathbf{H}} = \nabla \times \tilde{\mathbf{E}}. \quad (18b)$$

The converged solution to (18) can be decomposed as

$$\tilde{\mathbf{E}} = \sum_{k=1}^N \hat{\mathbf{E}}_{k,0} \cos(\omega_k t), \quad (19)$$

where $\hat{\mathbf{E}}_{k,0} = \Im\{\mathbf{E}_k\}$ gives the solution to the original frequency-domain problem (17) corresponding to ω_k . To obtain the “all k ” solution through EM-WaveHoltz is easy, the filtering operator simply needs to be modified as

$$\Pi\nu_E = \frac{2}{T} \int_0^T \left(\sum_{k=1}^N \cos(\omega_k t) - \frac{1}{4} \right) \tilde{\mathbf{E}}_\nu dt. \quad (20)$$

Here, the final time T is chosen such that $T/(\frac{2\pi}{\omega_k})$ is an integer for all k .

Once the EM-WaveHoltz iteration has converged to (19) we separate the different solutions by evolving (17) for one more T_k -period while applying the filters

$$\Im(\mathbf{E}_k) = \frac{2}{T_k} \int_0^{T_k} \left(\cos(\omega_k t) - \frac{1}{4} \right) \tilde{\mathbf{E}} dt, \quad (21)$$

$$\Re(\mathbf{E}_k) = \frac{2}{T_k} \int_0^{T_k} \sin(\omega_k t) \tilde{\mathbf{E}} dt. \quad (22)$$

II. DISCRETIZATION OF THE EM-WAVEHOLTZ METHOD

We have presented how the EM-WaveHoltz iteration converts a frequency-domain problem to a time-domain problem. In this section, we will use the Yee scheme [25], [26] and the discontinuous Galerkin (DG) method [3], [27], [28] as examples of integrating the EM-WaveHoltz iteration in existing time-domain solvers. We also want to point out that it is possible to couple the EM-WaveHoltz method to other type time-domain solvers such as spectral element method and continuous finite element method. Further, although we don't consider it here, our approach directly generalizes to linear dispersive frequency-domain models such as the generalized dispersive materials modeled through an auxiliary differential equation approach in [29].

A. Yee-EM-WaveHoltz

The Yee scheme [25], [26] or the finite-difference-time-domain (FDTD) method, is one of the most popular and successful methods in computational electromagnetics and can be easily turned into a fast FDFD method, the Yee-EM-WaveHoltz method, as follows.

For brevity we consider the two dimensional TM model, then $E_x = E_y = H_z = 0$. Assume a uniform time step size $\Delta t = T/M$ and denote a grid function at a point $(i\Delta x, j\Delta y, n\Delta t)$ by $F_{i,j}^n$ and denote $t^n = n\Delta t$. Then the Yee scheme to solve the time-domain problem in the EM-WaveHoltz formulation is:

$$\epsilon_{i,j} \frac{(\tilde{E}_z)_{i,j}^{n+1} - (\tilde{E}_z)_{i,j}^n}{\Delta t} = \left(\frac{(\tilde{H}_y)_{i+\frac{1}{2},j}^{n+\frac{1}{2}} - (\tilde{H}_y)_{i-\frac{1}{2},j}^{n+\frac{1}{2}}}{\Delta x} - \frac{(\tilde{H}_x)_{i,j+\frac{1}{2}}^{n+\frac{1}{2}} - (\tilde{H}_x)_{i,j-\frac{1}{2}}^{n+\frac{1}{2}}}{\Delta y} \right) - \sin(\omega t^{n+\frac{1}{2}}) (J_z)_{i,j} \quad (23a)$$

$$\frac{(\tilde{H}_x)_{i,j+\frac{1}{2}}^{n+\frac{1}{2}} - (\tilde{H}_x)_{i,j+\frac{1}{2}}^{n-\frac{1}{2}}}{\Delta t} = -\frac{1}{\mu_{i,j+\frac{1}{2}}} \frac{(\tilde{E}_z)_{i,j+1}^n - (\tilde{E}_z)_{i,j}^n}{\Delta y}, \quad (23b)$$

$$\frac{(\tilde{H}_y)_{i+\frac{1}{2},j}^{n+\frac{1}{2}} - (\tilde{H}_y)_{i+\frac{1}{2},j}^{n-\frac{1}{2}}}{\Delta t} = \frac{1}{\mu_{i+\frac{1}{2},j}} \frac{(\tilde{E}_z)_{i+1,j}^n - (\tilde{E}_z)_{i,j}^n}{\Delta x}, \quad (23c)$$

For the initial step $\tilde{H}_x^{-\frac{1}{2}}$ is initialized as

$$(\tilde{H}_x)_{i,j+\frac{1}{2}}^{-\frac{1}{2}} = (\tilde{H}_x)_{i,j+\frac{1}{2}}^0 - \frac{\Delta t}{2\mu_{i,j+\frac{1}{2}}} \left(-\frac{(\tilde{E}_z)_{i,j+1}^0 - (\tilde{E}_z)_{i,j}^0}{\Delta y} \right), \quad (24)$$

and $\tilde{H}_y^{-\frac{1}{2}}$ is initialized similarly.

To approximate the filter operator Π in (7) we use the composite trapezoidal rule

$$\Pi_h \begin{pmatrix} \nu_E \\ \nu_H \end{pmatrix} = \frac{2\Delta t}{T} \sum_{n=0}^M \eta_n \left(\cos(\omega t^n) - \frac{1}{4} \right) \begin{pmatrix} \tilde{\mathbf{E}}_\nu^n \\ \frac{\tilde{\mathbf{H}}_\nu^{n+\frac{1}{2}} + \tilde{\mathbf{H}}_\nu^{n-\frac{1}{2}}}{2} \end{pmatrix}, \quad (25)$$

where

$$\eta_n = \begin{cases} \frac{1}{2}, & n = 0 \text{ or } M, \\ 1, & \text{otherwise.} \end{cases} \quad (26)$$

Due to the second order time discretization, the solution obtained by the above iteration introduces an additional $O(\Delta t^2)$ error from time marching. Of course since $\Delta t \sim \min\{\Delta x, \Delta y\}$ the EM-WaveHoltz solution is converging at the same rate as the spatial discretization but nevertheless it does have an additional error. This error is easily eliminated by a small modification which we discuss next. We only present the 2D TM model here but note that EM-WaveHoltz can be straightforwardly generalized to the full 3D model.

B. Eliminating the temporal error in EM-WaveHoltz

For brevity we consider the energy conserving two dimensional TM model. To eliminate the time-marching error, we first slightly modify the source term in the time-domain. We replace $\sin(\omega t^{n+\frac{1}{2}})$ in (23a) with

$$S^{\frac{1}{2}} = \frac{\omega \Delta t}{2}, \quad S^{n+\frac{1}{2}} = S^{n-\frac{1}{2}} + \Delta t \omega \cos(\omega t^n). \quad (27)$$

Here, $S^{n+\frac{1}{2}}$ is a second order approximation to $\sin(\omega t^{n+\frac{1}{2}})$. Using $S^{n+\frac{1}{2}}$ instead of $\sin(\omega t^{n+\frac{1}{2}})$ gives us a chance to eliminate the error due to the time discretization.

Eliminating H_x and H_y in (23), we have

$$\begin{aligned} & \frac{(\tilde{E}_z)_{i,j}^{n+1} - 2(\tilde{E}_z)_{i,j}^n + (\tilde{E}_z)_{i,j}^{n-1}}{\Delta t^2} + L_h(\tilde{E}_z)_{i,j}^n \\ &= -\frac{1}{\epsilon_{i,j}}(J_z)_{i,j} \frac{S^{n+\frac{1}{2}} - S^{n-\frac{1}{2}}}{\Delta t} \\ &= -\frac{1}{\epsilon_{i,j}}(J_z)_{i,j} \omega \cos(\omega t^n), \end{aligned} \quad (28)$$

where

$$\begin{aligned} -L_h F_{i,j} &= \frac{1}{\epsilon_{i,j} \Delta x} \left(\frac{F_{i+1,j} - F_{i,j}}{\mu_{i+\frac{1}{2},j} \Delta x} - \frac{F_{i,j} - F_{i-1,j}}{\mu_{i-\frac{1}{2},j} \Delta x} \right) \\ &+ \frac{1}{\epsilon_{i,j} \Delta y} \left(\frac{F_{i,j+1} - F_{i,j}}{\mu_{i,j+\frac{1}{2}} \Delta y} - \frac{F_{i,j} - F_{i,j-1}}{\mu_{i,j-\frac{1}{2}} \Delta y} \right). \end{aligned} \quad (29)$$

(28) is an approximation to the second order form of the time-domain equation in EM-WaveHoltz. We now have the following theorem guaranteeing the convergence of the discrete iteration (for the energy conserving case)

Theorem 1. Let ν^∞ be the solution to

$$\tilde{\omega}^2 \nu^\infty - L_h \nu^\infty = \omega \left(\frac{1}{\epsilon} J \right), \quad (30)$$

where

$$\tilde{\omega} = \frac{\sin(\omega \Delta t / 2)}{\Delta t / 2} = \omega + O(\Delta t^2). \quad (31)$$

Further, let $\{-\lambda_j^2\}_{j=1}^N$ and $\{\psi_j\}_{j=1}^N$ be the eigenvalues and corresponding eigenfunctions of L_h , and $0 < \lambda_1 < \lambda_2 < \dots < \lambda_N$. Assume that ω is not a resonance and denote the relative distance to the closest resonance

$$\delta_h = \min_j |\lambda_j - \omega| / \omega > 0. \quad (32)$$

Then, for the energy conserving method (23), with the filter (25), the Yee-EM-WaveHoltz iteration $\nu^{(k+1)} = \Pi_h \nu^{(k)}$ with $\nu^{(0)} = 0$ converges to ν^∞ as long as

$$\Delta t \leq \frac{2}{\lambda_N + 2\omega/\pi}, \quad \omega \Delta t \leq \min(\delta_h, 1). \quad (33)$$

Moreover, the convergence rate is at least $\rho_h = \max(1 - 0.3\delta_h^2, 0.6)$.

The proof of this Theorem is presented in Appendix C. We note that the first constraint on the timestep is essentially the standard CFL condition for an explicit method while the second condition could be very strict. In fact, for all our numerical experiments, we only choose the Δt based on the CFL condition, and the violation of the second condition does not lead to problems. Hence, we conjecture that the second condition is not a practical limitation.

Now, if we replace $\cos(\omega t^n)$ with $\cos(\bar{\omega} t^n)$ in (27) with

$$\bar{\omega} = \frac{2}{\Delta t} \sin^{-1} \left(\frac{\omega \Delta t}{2} \right), \quad (34)$$

and modify the trapezoidal weights in the filter as

$$\hat{\Pi}_h \nu = \frac{2\Delta t}{T} \sum_{n=0}^M \left(\cos(\omega t^n) - \frac{1}{4} \right) \frac{\cos(\omega t^n)}{\cos(\bar{\omega} t^n)} \tilde{E}_z^n. \quad (35)$$

Then Theorem 1 holds but the convergence is to ν^∞ being the solution to the standard discretized frequency-domain problem

$$\omega^2 \nu^\infty - L_h \nu^\infty = \omega \left(\frac{1}{\epsilon} J \right). \quad (36)$$

The derivation of this strategy is discussed in Appendix D along with the proof of Theorem 1. An alternative strategy to eliminate the temporal error is suggested in [30].

C. DG-EM-WaveHoltz

The discontinuous Galerkin (DG) method, due to its high order accuracy, flexibility to use nonconforming meshes and its suitability for parallel implementation, has become increasingly popular for the simulation of time-domain wave propagation. As for the Yee scheme, DGTD can easily be turned into a frequency-domain solver using our approach. Here we use the time-domain DG method of [3], [27].

Consider Maxwell's equation in d -dimensions. Let Ω_j be an element, and $P^s(\Omega_j)$ be the space of polynomials at most degree s . Define $V_h^s(\Omega_j) = (P^s(\Omega_j))^d$ to be the corresponding vector polynomial space. The DG method seeks the solution $\mathbf{E}_h \in V_h^s(\Omega_j)$, $\mathbf{H}_h \in V_h^s(\Omega_j)$ such that for any $\phi \in V_h^s(\Omega_j)$, $\psi \in V_h^s(\Omega_j)$

$$\begin{aligned} \int_{\Omega_j} \partial_t \tilde{\mathbf{E}}_h \cdot \phi d\mathbf{V} &= \int_{\Omega_j} \tilde{\mathbf{H}}_h \cdot \nabla \times \left(\frac{1}{\epsilon} \phi \right) d\mathbf{V} \\ &+ \int_{\partial\Omega_j} (\hat{\mathbf{H}} \times \mathbf{n}) \cdot \left(\frac{1}{\epsilon} \phi \right) ds - \int_{\Omega_j} \sin(\omega t) \mathbf{J} \cdot \phi d\mathbf{V}, \end{aligned} \quad (37a)$$

$$\begin{aligned} \int_{\Omega_j} \partial_t \tilde{\mathbf{H}}_h \cdot \psi d\mathbf{V} &= - \int_{\Omega_j} \tilde{\mathbf{E}}_h \cdot \nabla \times \left(\frac{1}{\mu} \psi \right) d\mathbf{V} \\ &- \int_{\partial\Omega_j} (\hat{\mathbf{E}} \times \mathbf{n}) \cdot \left(\frac{1}{\mu} \psi \right) ds. \end{aligned} \quad (37b)$$

TABLE I
COMPUTATIONAL TIME (SEC)

	N	$\omega = \omega_0$	$\omega = 2.24\omega_0$	$\omega = 2.7\omega_0$
EM-WH	120	20	12	12
	240	94	55	60
	480	562	326	350
MEEP	120	11	21	34.14
	240	109	180	229
	480	1095	1531	2000

Here, \mathbf{n} is the outward pointing normal of a face and $\hat{\mathbf{H}}$ and $\hat{\mathbf{E}}$ are numerical fluxes. A stable and accurate choice for the numerical fluxes is

$$\hat{\mathbf{H}} = \{\tilde{\mathbf{H}}\} + \alpha[\tilde{\mathbf{E}}], \quad \hat{\mathbf{E}} = \{\tilde{\mathbf{E}}\} + \beta[\tilde{\mathbf{H}}]. \quad (38)$$

Here \mathbf{v}^\pm denotes the two values on each side of a face, $\{\mathbf{v}\} = \frac{1}{2}(\mathbf{v}^+ + \mathbf{v}^-)$ is the average and $[\mathbf{v}] = \mathbf{n}^+ \times \mathbf{v}^+ + \mathbf{n}^- \times \mathbf{v}^-$ is the jump. The semi-discretization (37) can be evolved in a method of lines fashion, using for example a Runge-Kutta or Taylor method as the time stepper. Depending on the time discretization it may be possible to eliminate the time error as discussed above but we don't pursue this here. Further, in the examples below we always use the trapezoidal rule to discretize the filter.

III. NUMERICAL RESULTS

In this section we demonstrate the performance of the EM-WaveHoltz methods on several examples in two and three dimensions. The sin-forcing formulation is used in two dimensions and the cos-forcing formulation is used in three dimensions, unless otherwise specified. For all numerical examples, the time step size Δt is chosen based on the CFL conditions of the time-domain methods. Again we note that such timesteps violates the second condition in Theorem 1 but that this condition appears to be a technicality as none of the examples below are affected by this. In this section we always use the Krylov accelerated version of the iteration.

A. Comparison with the MEEP FDFD solver

We compare our Yee-EM-WaveHoltz code with the iterative FDFD solver of the open source C++ package MEEP [31]. Our code is implemented by combining EM-WaveHoltz with the FDTD code of the C library rbcpack [32]. Our code uses a self-implemented GMRES solver without restart. The FDFD solver of MEEP uses BICG-Stab(l) method [33]. Both codes are executed in a serial-manner on a 2015 MacBook with 2.2 GHz Quad-Core Intel Core i7 cpu.

Following MEEP package's benchmark example for the FDFD code (see [34]), we consider a ring resonator and the 2D TM model. The computational domain is $[-6, 6]^2$ with nonreflecting boundary conditions. A ring resonator with $\epsilon_r = 3.4^2$ is located at $\{(x, y) : 1 \leq \sqrt{x^2 + y^2} \leq 2\}$. The permittivity outside the ring is $\epsilon = 1$, and the permeability $\mu = 1$ in the whole computational domain. Two point sources are placed at $(1.1, 0)$ with magnitude 1 and $(-1.1, 0)$ with magnitude -1 . Let $\omega_0 = 0.118 \times 2\pi$. We consider $\omega = \omega_0, 2.24\omega_0$ and $2.7\omega_0$. We use $N = 120, 240$ and 480 grids in each direction.

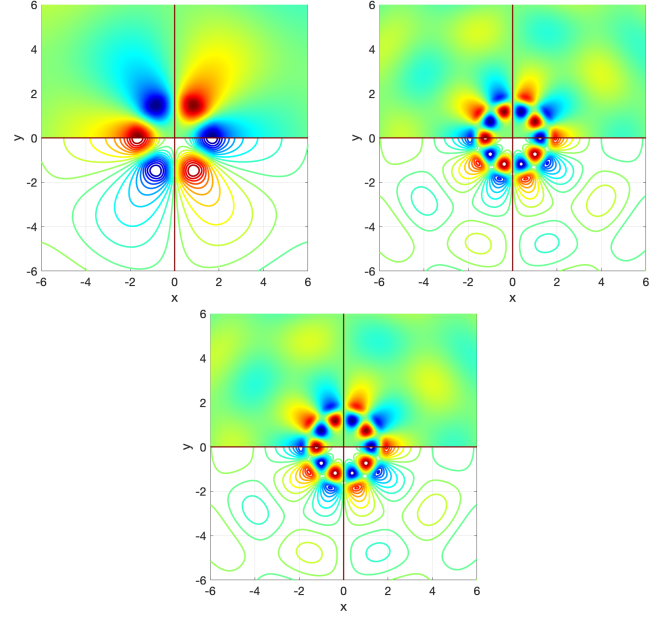


Fig. 1. The real part of the E_z field (normalized). Top left figure, $\omega = \omega_0$, top right figure $\omega = 2.24\omega_0$, bottom figure: $\omega = 2.7\omega_0$. Left: Yee-EM-WaveHoltz. Right: MEEP's FDFD solver. .

TABLE II
TOTAL NUMBER OF ITERATIONS WITH 10^{-7} RELATIVE RESIDUAL

	N	$\omega = \omega_0$	$\omega = 2.24\omega_0$	$\omega = 2.7\omega_0$
EM-WH	120	8	11	14
	240	8	11	15
	480	8	11	15
BICG-Stab(l)	120	144	256	405
	240	280	449	557
	480	586	800	1092

For both solvers, we set the relative tolerance as 10^{-7} . For the Yee-EM-WaveHoltz, we use cos-forcing and filter over 10 periods. To obtain convergent results for all frequencies, we use $l = 10$ in the BICG-Stab(l) FDFD solver. In the results displayed in Figure 1, we observe that the EM-WaveHoltz and the FDFD agree well. Table I presents the computational time needed. The Yee-EM-WaveHoltz code is always faster except for ω_0 and $N = 120$. Its advantage increases with mesh refinement and the size of the frequency. In Table II, we present the total number of iterations needed for convergence. The Yee-EM-WaveHoltz always needs fewer iterations for convergence. Moreover, for a fixed frequency, the number of iteration needed by Yee-EM-WaveHoltz almost does not grow as the grid is refined, while the BICG-Stab(10) needs more iterations.

B. Comparison with a direct FDFD solver

Sparse multifrontal direct FDFD solvers are fast, however, for the full 3D problem and with increasing frequency such solvers quickly become too large to fit in memory. To demonstrate this we consider a 3D problem with $\omega = 12.5$, PEC boundary conditions and a source $J_x = \omega y(y-1)z(z-1) + \frac{2}{\omega}(y(y-1) + z(z-1))$, $J_y = \omega x(x-1)z(z-1) + \frac{2}{\omega}(x(x-1) + z(z-1))$ and $J_z = \omega x(x-1)y(y-1) + \frac{2}{\omega}(x(x-1) + y(y-1))$.

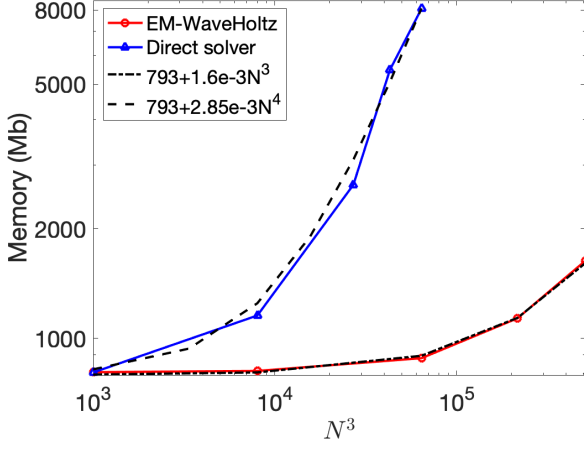


Fig. 2. Peak memory for EM-WaveHoltz and a direct solver based on sparse multifrontal LU factorization for a 3D problem with PEC boundary conditions

We use N grid points in each direction. We implement an Yee-EM-WaveHoltz code and a direct FDFD code in Julia. Both codes share exactly the same spatial discretization subroutines based on sparse matrices. GMRES solver with relative tolerance 10^{-8} is applied in the EM-WaveHoltz code. The direct solver uses Julia's sparse multifrontal LU factorization, which calls SuiteSparse [35]. As shown in Figure 2, we observe that the peak memory needed by the EM-WaveHoltz scales roughly as $O(DOF) = O(N^3)$, and the peak memory needed by the direct solver scales roughly as $O(DOF^{4/3}) = O(N^4)$.

C. Grid convergence of Yee-EM-WaveHoltz

We consider the 2D TM model and non-dimensionalize the equations so that $\epsilon = \mu = 1$ and manufacture a forcing

$$J = 16\omega x^2(x-1)^2y^2(y-1)^2 + \frac{32}{\omega} \left((6x^2 - 6x + 1)y^2(y-1)^2 + (6y^2 - 6y + 1)x^2(x-1)^2 \right)$$

so that the exact solution is $E_z(x, y) = 16x^2(x-1)^2y^2(y-1)^2$. This solution is compatible with perfect electric conductor (PEC) boundary conditions on the domain $[0, 1]^2$. We apply the Yee scheme and the EM-WaveHoltz iteration with GMRES acceleration. The relative tolerance of the GMRES solver is set as 10^{-10} .

To test the convergence for a) one frequency in one solve, and b) multiple frequencies in one solve, we perform a grid refinement study at fixed frequencies $\omega_1 = 5.5$, $3\omega_1$ and $7\omega_1$. In Figure 3, without eliminating the temporal error, we display how the error is decreased as the grid size is reduced. As expected, for both of one frequency in one solve and multiple frequencies in one solve, we observe second order convergence. For the same frequency and the same mesh, the magnitude of the errors for one frequency and multiple frequencies in one solve are close to each other.

We also use this example to investigate the influence of the temporal error in the EM-WaveHoltz method. In Table III, due to the temporal error, we observe that the error of the direct FDFD solver is smaller than the Yee-EM-WaveHoltz for for

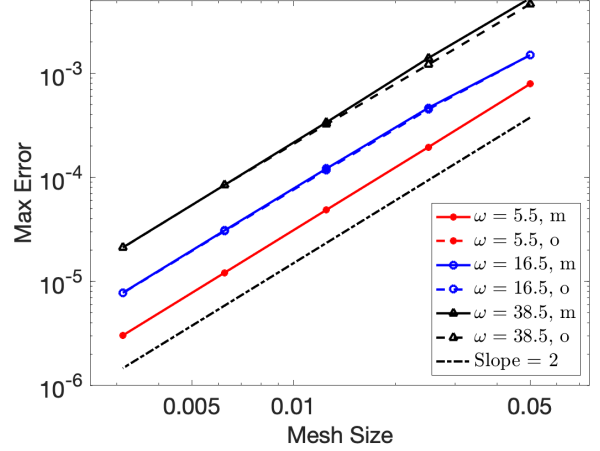


Fig. 3. Grid convergence of a manufactured solution. Here “o” stands for one frequency in one solve, and “m” stands for multiple frequencies in one solve. The errors displayed are for E_z for a 2D TM model.

$\omega = 16.5$ and $\omega = 37.5$, but slightly bigger for $\omega = 5.5$. For $\omega = 5.5$, it is likely that the sign for the temporal error and the spatial error are different.

Finally, we verify the effectiveness of our strategy to eliminating the temporal error. As shown in Table IV, the difference between the FDFD solution and the Yee-EM-WaveHoltz solution after eliminating temporal error are at most $O(10^{-12})$, which is much smaller than the numerical error.

TABLE III
ERRORS FOR THE MANUFACTURE SOLUTION OF 2D TM MODEL WITH $N = 160$ GRIDS IN EACH DIRECTION.

ω	5.5	16.5	35.5
EM-WH with temporal error	1.21e-5	3.09e-5	8.45e-5
Direct-FDFD	1.73e-5	2.24e-6	2.26e-7

TABLE IV
DIFFERENCE BETWEEN YEE-EM-WAVEHOLTZ SOLUTION AFTER ELIMINATING THE TEMPORAL ERROR AND THE FDFD SOLUTION WITH $N = 160$ GRIDS IN EACH DIRECTION

ω	5.5	16.5	37.5
Difference	7.38e-15	9.22e-14	2.24e-12

D. Plane wave scattering and p -convergence of DG-EM-WaveHoltz

Next we combine the EM-WaveHoltz iteration with the upwind nodal discontinuous Galerkin method [3]. We consider the 2D TM-model and the scattering wave from a PEC disk due to the incident plane wave $E_z^{\text{inc}} = e^{-i\omega x}$ with $\omega = 15$. The radius of the disk is $a = 0.25$. The exact solution of this problem is a Mie series (see e.g. [36]), and is presented in Fig. 4). The incident wave is imposed by setting the boundary value E_z^{bc} equal to the exact solution. In the EM-WaveHoltz formulation, the boundary condition of the time-domain problem is defined as $\Re\{E_z^{bc}\} \cos(\omega t) + \Im\{E_z^{bc}\} \sin(\omega t)$. With this choice, one can show that the EM-WaveHoltz converges to the real part of the frequency-domain solution. For a p -th degree

polynomial spatial discretization we use a $p+1$ -th order Taylor series method in time and filter over 5 periods.

We perform a p -convergence study with the unstructured mesh in Fig. 4. The maximum error and the number of iterations for convergence with relative tolerance 10^{-8} are shown in Table V. As the polynomial order p increases, the error decays, and high order schemes achieves $O(10^{-6})$ error on this relatively coarse mesh. As the polynomial order p increases, number of points per wavelength grows, but the total number of iterations for convergence does not grow.

TABLE V
MAXIMUM ERROR AND THE TOTAL NUMBER OF ITERATIONS FOR THE SCATTERING WAVE FROM A PEC DISK, WITH DG-EM-WAVEHOLTZ AND p -TH ORDER POLYNOMIAL

p	3	4	5	6	7	8
Error	2.86e-2	4.65e-3	6.89e-4	6.40e-5	7.89e-6	1.37e-6
Iterations	45	39	38	38	37	37

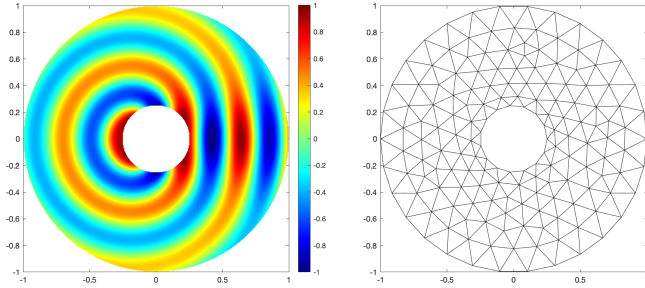


Fig. 4. Left figure: exact solution for $\omega = 15.0$ of the scattering problem. Right figure: Unstructured mesh.

E. Plane wave scattering with incident fields and Yee scheme

We consider the same plane wave scattering problem as Section III-D with the incident plane wave $E_z^{\text{inc}} = e^{-i\omega x}$ and $\omega = 15$. To show the capability of using a field source, we apply the Yee-EM-WaveHoltz method and impose the incident fields following the total field/scattered field formulation in [2]. We split the computational domain into a total field region $[-0.5, 0.5]^2$ and a scattered field region. The incident wave is imposed through the interface condition between the two regions, and the double absorbing boundary layer (DAB) by Hagstrom et al. [37] is applied to impose the nonreflecting boundary conditions. The setup of the Yee scheme is illustrated in the left figure of Fig. 5. To impose the right going incident wave, we follow similar arguments to (5) and define the corresponding time-domain incident fields as

$$\begin{aligned}\tilde{\mathbf{E}}_z^{\text{inc}} &= \cos(\omega x) \sin(\omega t) - \sin(\omega x) \cos(\omega t) \\ &= \sin(\omega(t - x)) = \Im\{e^{i\omega(t-x)}\}, \\ \tilde{\mathbf{H}}_x^{\text{inc}} &= 0, \quad \tilde{\mathbf{H}}_y^{\text{inc}} = -\tilde{\mathbf{E}}_z^{\text{inc}}.\end{aligned}\quad (39)$$

We use a 401×401 uniform mesh, and set the relative tolerance of the GMRES solver as 10^{-8} . The numerical solution matches the exact solution very well (see right figure of Fig. 5).

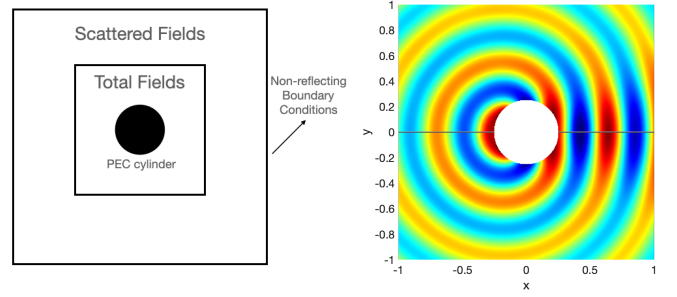


Fig. 5. Left figure: the set-up of the total field/scattered field formulation. Right figure: the real part of the scattered wave with $\omega = 15$, numerical solution on the top and exact solution on the bottom.

F. Number of iterations for different frequencies and boundary conditions in two dimensions

In this experiment we solve the 2D TM model with the source

$$J_z = -\omega \exp(-\sigma((x - 0.01)^2 + (y - 0.015)^2)), \quad (40)$$

where $\sigma = \max(36, \omega^2)$, $\epsilon = \mu = 1$, and the computational domain is $[-1, 1]^2$. Here we sweep over the frequencies $\omega = k + \frac{1}{2}$, $1 \leq k \leq 100$. We use the GMRES accelerated Yee-EM-WaveHoltz iteration and to keep the solution reasonably well resolved we use $8\lceil\omega\rceil$ grids in each directions, where $\lceil\omega\rceil$ is the smallest integer larger than ω .

We solve this problem with 6 different boundary conditions: (1) 4 open boundaries, (2) 1 PEC boundary and 3 open boundaries, (3) 2 parallel PEC boundaries and 2 open boundaries, (4) 2 PEC boundaries next to each other forming a PEC corner and 2 open boundaries, (5) 3 PEC boundaries and 1 open boundary, (6) 4 PEC boundaries. The rationale here is that in problems (1), (2) and (4) there will not be any opposing PEC walls where waves can be “trapped” while in the other three problems there are.

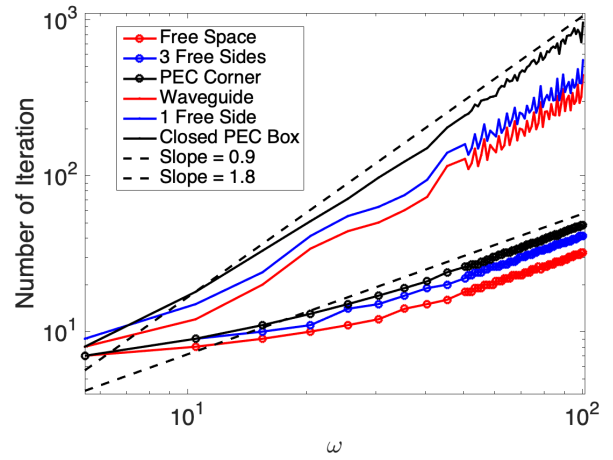


Fig. 6. Number of iterations as a function of frequency for the six different 2D TM problems.

We also note that in the open directions we employ the optimally accurate double absorbing boundary layer (DAB) by Hagstrom et al. [37]. The order of approximation in the DAB

layers we use is 10 which virtually makes the non-reflecting boundary conditions exact.

In the EM-WaveHoltz iteration, we use 10 periods so that $T = 10 \frac{2\pi}{\omega}$. This reduces the memory consumption in GMRES by a factor 10 and reduces the number of iterations by nearly a factor of 10 (the cost per iteration of course goes up by 10 as well). In Fig. 6, the number of iteration required to reduce the relative residual below 10^{-7} are presented. We observe that for the problems without trapped waves, the number of iterations scales approximately as $\omega^{0.9}$. For the problems with trapped waves, the iteration converges slower and the number of iterations scales as approximately $\omega^{1.8}$.

G. Number of iterations for different frequencies and boundary conditions in three dimensions

In this example we solve the 3D Maxwell's equation with a source

$$J_x = -\omega \exp(-\sigma(x^2 + y^2 + z^2)), \quad J_y = J_z = 0. \quad (41)$$

Here $\sigma = \max(36, \omega^2)$, $\epsilon = \mu = 1$ and the computational domain is $[-1, 1]^3$.

To measure how the number of iterations grow with the frequency, three different problems are considered: (1) an open domain, (2) two parallel PEC plates, (3) five PEC boundaries and one free side on the most left side. Again, we still apply the highly accurate double absorbing boundary layer (DAB) for non-reflecting boundary conditions. The order of the DAB layers is set as 5 guaranteeing that the error of the non-reflecting boundary conditions is well below the discretization error.

We sweep over frequencies and use the GMRES accelerated Yee-EM-WaveHoltz method with the cos-forcing. To have a well resolved solution we use $4\lceil\omega\rceil$ elements in each direction, where $\lceil\omega\rceil$ is the smallest integer larger than ω . In the EM-WaveHoltz iteration, we set T as 5 periods.

In Figure 7, iteration numbers to reduce the relative residual below 10^{-6} are presented. The total number of iterations is estimated to scale as $\omega^{0.9}$ for the open problem, $\omega^{1.9}$ for the parallel PEC plate problem and $\omega^{2.5}$ for the problem with one free side.

We also use the the sin-forcing to simulate the open domain problem with the same mesh and the error tolerance. We observe that the number of iteration is exactly the same as the cos-forcing, though the relative residual is slightly different for high frequencies.

H. Number of iterations for different points per wavelength

TABLE VI

NUMBER OF ITERATIONS FOR DIFFERENT NUMBER OF POINTS PER WAVELENGTH, 2D-TM MODEL, $\lceil\omega\rceil = \text{CEIL}(\omega)$.

Boundaries	N	$2\lceil\omega\rceil$	$4\lceil\omega\rceil$	$6\lceil\omega\rceil$	$8\lceil\omega\rceil$
open	$\omega = 12.5$	9	9	9	9
PEC	$\omega = 12.5$	11	11	11	11
open	$\omega = 25.5$	13	12	12	12
PEC	$\omega = 25.5$	25	24	24	24

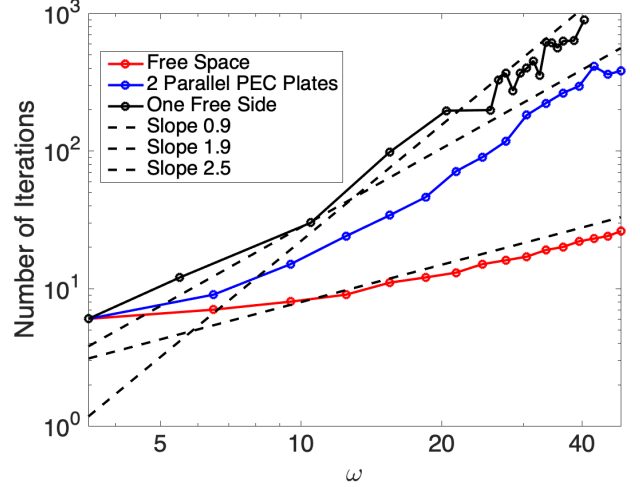


Fig. 7. Number of iterations as a function of frequency for different 3D problems.

Here, we fix the frequency and more systematically investigate the number of iterations needed for convergence for different number of grid points per wavelength. We use the Yee-EM-WaveHoltz method with GMRES acceleration, and $\epsilon = \mu = 1$ is considered. For the 2D-TM model, we consider the computational domain $[-1, 1]^2$ and the source

$$J_z = \omega \exp(-144(x^2 + y^2)), \quad (42)$$

with either 4 open boundaries or 4 PEC boundaries. For the 3D model, we consider the computational domain $[-1, 1]^3$ and the source

$$J_x = -\omega \exp(-144(x^2 + y^2 + z^2)), \quad J_y = J_z = 0, \quad (43)$$

with either 6 open boundaries or 6 PEC boundaries. In each direction, we use $N + 1$ grid points. We take $T = 10 \frac{2\pi}{\omega}$. The stopping criteria is that the relative residual falls below 10^{-8} for the 2D TM-model and 10^{-5} for the 3D model.

The results are presented in Table VI and Table VII. When considering an open problem at a fixed frequency, we observe that the number of iterations does not change as the number of grid points per wavelength is increased. For the PEC problem in three dimensions the number of iterations are reduced slightly as the resolution is increased and for the 2D PEC problem it does not change significantly. Based on this experiment and other experiments, our observation is that the algorithm is robust with respect to resolution (but of course the discretization error will depend on the resolution.)

TABLE VII

NUMBER OF ITERATIONS FOR DIFFERENT NUMBER OF POINTS PER WAVELENGTH, 3D.

Boundaries	N	$2\lceil\omega\rceil$	$4\lceil\omega\rceil$	$6\lceil\omega\rceil$	$8\lceil\omega\rceil$
open	$\omega = 12.5$	5	5	5	6
PEC	$\omega = 12.5$	26	24	23	22
open	$\omega = 25.5$	7	7	7	7
PEC	$\omega = 25.5$	174	153	150	135

I. Smaller Krylov subspaces by longer filter time

As we mentioned before, we can filter over multiple periods $T = N \frac{2\pi}{\omega}$, which allows the further propagation of the wave. We consider $T = N \frac{2\pi}{\omega}$ with $N = 1, 3, 5$ for 2D and 3D open domain problem. The setup of this test is the same as Section III-F for 2D and Section III-G for 3D. We scan over different frequencies and apply the GMRES accelerated Yee-EM-WaveHoltz. The total number of iteration allowed is set as 200 in 2D and 100 in 3D. As can be seen in Figure 8 for high frequencies both the 2D and the 3D solver, when using $T = \frac{2\pi}{\omega}$, fails to converge to the desired tolerance before reaching the maximum number of iterations.

In Figure 8, we present unscaled number of iterations against the frequency and observe that the number of iterations decays as the propagation time T in the time-domain grows. To further quantify the relation between the computational cost and $T = N \frac{2\pi}{\omega}$, we scale the number of iterations by N and present the result in Figure 9. We observe that for $N = 3$ and 5 the scaled curves collapse, implying that the total computational time is approximately the same. Thus, without increasing the computational cost, filtering over longer time can decrease the number of iterations, which in turn reduces the size of the Krylov subspace used by GMRES.

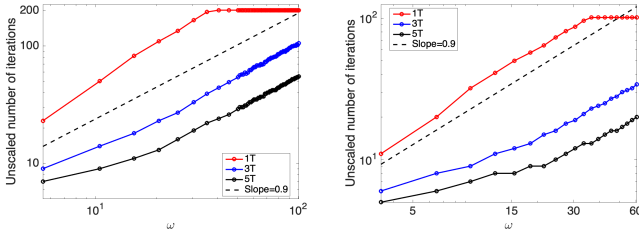


Fig. 8. Unscaled number of iterations as a function of frequency for different filtering time. Top: 2D open problem. Bottom: 3D open problem.

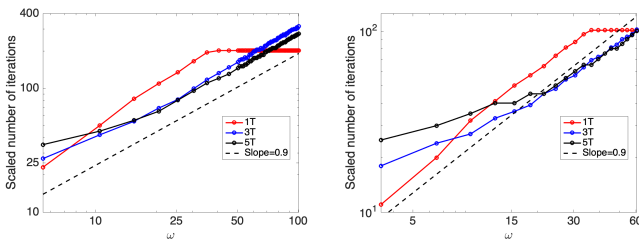


Fig. 9. Scaled number of iterations = $N \times$ number of iterations, if $T = N \frac{2\pi}{\omega}$. Scaled number of iterations as a function of frequency for different filtering time. Top: 2D open problem. Bottom: 3D open problem.

J. SPD structure and condition numbers for energy conserving 2D TM-model

Here, we consider the 2D TM model with PEC boundary conditions, $\epsilon = \mu = 1$, $\omega = 10$ and the Gaussian source

$$J_z = -\omega \exp(-\omega^2(x^2 + y^2)), \quad (44)$$

on the computational domain $[-1, 1]^2$. We apply the Yee-EM-WaveHoltz method, and filter over 10 periods in the time-domain. We use this example to verify that our method results

in a SPD linear system. The code is implemented in a matrix free manner. The matrix $I - S$ is constructed column by column through the calculation of matrix-vector multiplication $(I - S)e_i$ where e_i is a column vector whose i -th element is 1 and all other elements are 0.

We use $N = 10, 20, \dots, 100$ elements in each direction. We first compare $I - S$ and $(I - S)^T$. The L_∞ norm of their difference is always on the level of machine accuracy. The smallest eigenvalue of the resulting linear system is always positive. Moreover, when N is large enough to resolve the wave structure, the condition number of the resulting matrix does not increase as N grows. The condition numbers are 79.1305 for $N = 90$, 75.5935 for $N = 95$ and 72.7603 for $N = 100$. This matches our previous observation that the total number of iterations does not grow with increased number of points per wavelength.

IV. CONCLUSION

In this paper, we proposed the EM-WaveHoltz method, which converts the frequency-domain problem into a time-domain problem with time periodic forcing. The main advantages of the proposed method are as follows.

- 1) The resulting linear system is positive definite, and the GMRES iterative solver converges reasonably fast even though no preconditioning was used.
- 2) The method is flexible and straightforward to implement, it only requires a time-domain solver. In this paper, we illustrated how either the classical Yee scheme or a discontinuous Galerkin method can be used to construct frequency-domain solvers.
- 3) A unique feature of our EM-WaveHoltz method is that the solution to multiple frequencies can be obtained in a single solve.

Potential future research directions are to design preconditioning strategies to further accelerate the convergence of the proposed iterative method. It would also be interesting to apply the method to more advanced dispersive material models.

APPENDIX A

DERIVATION OF THE EM-WAVEHOLTZ ITERATION WITH COS-FORCING

The real valued $T = 2\pi/\omega$ -periodic solutions to (10) is in the form:

$$\tilde{\mathbf{E}} = \hat{\mathbf{E}}_0 \cos(\omega t) + \hat{\mathbf{E}}_1 \sin(\omega t), \quad (45)$$

$$\tilde{\mathbf{H}} = \hat{\mathbf{H}}_0 \cos(\omega t) + \hat{\mathbf{H}}_1 \sin(\omega t). \quad (46)$$

Matching the $\sin(\omega t)$ and $\cos(\omega t)$ term, we reach

$$\begin{aligned} \epsilon\omega(-\hat{\mathbf{E}}_0) &= \nabla \times \hat{\mathbf{H}}_1, \\ \epsilon\omega(\hat{\mathbf{E}}_1) &= \nabla \times \hat{\mathbf{H}}_0 - \mathbf{J}, \\ \mu\omega(-\hat{\mathbf{H}}_0) &= -\nabla \times \hat{\mathbf{E}}_1, \\ \mu\omega(\hat{\mathbf{H}}_1) &= -\nabla \times \hat{\mathbf{E}}_0. \end{aligned}$$

Based on (2), it follows that

$$\hat{\mathbf{E}}_0 = \Re\{E\}, \quad \hat{\mathbf{H}}_0 = \Re\{H\}, \quad \hat{\mathbf{E}}_1 = -\Im\{E\}, \quad \hat{\mathbf{H}}_1 = -\Im\{H\}.$$

By construction, one can further verify that $\Pi(\Im\{\mathbf{E}\}, \Im\{\mathbf{H}\})^T = (\Re\{\mathbf{E}\}, \Re\{\mathbf{H}\})^T$.

APPENDIX B ANALYSIS OF ENERGY CONSERVING EM-WAVEHOLTZ ITERATION

Similar to [1], we analyze the convergence of the simplified EM-WaveHoltz iteration for the energy conserving case and show that $I - S$ is a self-adjoint positive definite operator.

Eliminating \mathbf{H} in the frequency-domain equation (1), we have

$$-\omega^2 \epsilon \mathbf{E} = -\nabla \times \left(\frac{1}{\mu} \nabla \times \mathbf{E} \right) - i\omega \mathbf{J}. \quad (47)$$

With the real-valued current source J , we further have

$$-\epsilon \omega^2 \Im(\mathbf{E}) = -\nabla \times \left(\frac{1}{\mu} \nabla \times \Im(\mathbf{E}) \right) - \omega \mathbf{J}. \quad (48)$$

Eliminating $\tilde{\mathbf{H}}$ in the time-domain equation (4), we obtain

$$\epsilon \partial_{tt} \tilde{\mathbf{E}} = -\nabla \times \left(\frac{1}{\mu} \nabla \times \tilde{\mathbf{E}} \right) - \omega \cos(\omega t) \mathbf{J}, \quad (49)$$

with $\tilde{\mathbf{E}}|_{t=0} = \nu_E$ and $\tilde{\mathbf{E}}_t = \mathbf{0}$.

Suppose there is an orthonormal basis of $L^2(\Omega)$ consisted by the eigenfunctions of the operator $-\frac{1}{\epsilon} \nabla \times \left(\frac{1}{\mu} \nabla \times \right)$ (For example this holds under the assumptions of Theorem 8.2.4 in [38]). Let the eigenfunctions $\{\phi_j\}_{j=1}^\infty$ consist an orthonormal basis of the L^2 space. Let $\{-\lambda_j^2\}_{j=1}^\infty$ denote the corresponding nonpositive eigenvalues. For simplicity of notations, we let $\nu_E = \nu$. Then, \mathbf{E} , $\tilde{\mathbf{E}}$, \mathbf{J} , ν can be expanded as:

$$\begin{aligned} \mathbf{E} &= \sum_{j=1}^\infty \mathbf{E}_j \phi_j, \quad \tilde{\mathbf{E}} = \sum_{j=1}^\infty \tilde{\mathbf{E}}_j \phi_j, \\ \mathbf{J} &= \sum_{j=1}^\infty \mathbf{J}_j \phi_j, \quad \nu = \sum_{j=1}^\infty \nu_j \phi_j. \end{aligned} \quad (50)$$

Solve (47) and (49):

$$\mathbf{E}_j = \frac{\frac{1}{\epsilon} \omega \mathbf{J}_j}{\lambda_j^2 - \omega^2}, \quad (51)$$

$$\tilde{\mathbf{E}}_j = \mathbf{E}_j (\cos(\omega t) - \cos(\lambda_j t)) + \nu_j \cos(\lambda_j t). \quad (52)$$

Then,

$$\Pi \nu = \sum_{j=1}^\infty \bar{\nu}_j \phi_j, \quad \bar{\nu}_j = (1 - \beta(\lambda_j)) \mathbf{E}_j + \beta(\lambda_j) \nu_j, \quad (53)$$

where

$$\beta(\lambda) = \frac{2}{T} \int_0^T \left(\cos(\omega t) - \frac{1}{4} \right) \cos(\lambda t) dt. \quad (54)$$

Realizing that

$$\begin{aligned} \Pi \mathbf{0} &= \sum_{j=1}^\infty ((1 - \beta(\lambda_j)) \mathbf{E}_j + \beta(\lambda_j) \mathbf{0}) \\ &= \sum_{j=1}^\infty (1 - \beta(\lambda_j)) \mathbf{E}_j, \end{aligned} \quad (55)$$

we have

$$S \sum_{j=1}^\infty \nu_j \phi_j = \Pi \nu - \Pi \mathbf{0} = \sum_{j=1}^\infty \beta(\lambda_j) \nu_j \phi_j. \quad (56)$$

Furthermore, as proved in [1], the spectral radius ρ of S is strictly smaller than 1:

$$\rho \sim 1 - 6.33\delta^2, \quad \delta = \inf_j \frac{\lambda_j - \omega}{\omega}. \quad (57)$$

As a result, when ω is not a resonance,

$$\lim_{n \rightarrow \infty} (\Pi \nu^n - \mathbf{E}) = \lim_{n \rightarrow \infty} S^n (\nu^0 - \mathbf{E}) \rightarrow 0. \quad (58)$$

Furthermore,

$$((I - S)\nu, \nu) \geq (1 - \rho) \|\nu\|^2 > 0. \quad (59)$$

This also verifies that $I - S$ is positive definite. One can easily verify that $I - S$ is self-adjoint based on the expansion (56).

APPENDIX C PROOF OF THEOREM 1

Proof of Theorem 1. Proof of Theorem 1 is similar to the proof of Theorem 2.4 of [1]. Here, we only point out the key steps. We expand all functions as

$$\begin{aligned} \tilde{E}_z^n &= \sum_{j=1}^N (\tilde{E}_z)_j^n \psi_j, \quad J_z = \sum_{j=1}^N (J_z)_j \psi_j, \\ (E_z) &= \sum_{j=1}^N (E_z)_j \psi_j, \quad \nu^\infty = \sum_{j=1}^N \nu_j^\infty \psi_j. \end{aligned} \quad (60)$$

Then,

$$(E_z)_j = \frac{\frac{1}{\epsilon} \omega (J_z)_j}{\omega^2 - \lambda_j^2}, \quad \nu_j^\infty = \frac{\frac{1}{\epsilon} \omega (J_z)_j}{\tilde{\omega}^2 - \lambda_j^2}. \quad (61)$$

Moreover, for $n \neq 0$

$$\begin{aligned} &(\tilde{E}_z)_j^{n+1} - 2(\tilde{E}_z)_j^n + (\tilde{E}_z)_j^{n-1} + \Delta t^2 \lambda_j^2 (\tilde{E}_z)_j^n \\ &= -\omega \Delta t^2 \cos(\omega t^n) \frac{1}{\epsilon} J_z, \end{aligned} \quad (62)$$

and

$$(\tilde{E}_z)_j^0 = \nu_j, \quad (\tilde{E}_z)_j^1 = (1 - \frac{1}{2} \lambda_j^2 \Delta t^2) \nu_j - \frac{\omega}{2} \Delta t^2 \left(\frac{1}{\epsilon} J_z \right)_j. \quad (63)$$

Following Appenndix B of [1], one can verify that

$$(\tilde{E}_z)_j^n = (\nu_j - \nu_j^\infty) \cos(\tilde{\lambda}_j t^n) + \nu_j^\infty \cos(\omega t^n), \quad (64)$$

where

$$\frac{\sin(\tilde{\lambda}_j \Delta t / 2)}{\Delta t / 2} = \lambda_j. \quad (65)$$

Let $\Pi_h \nu = \sum_j \bar{\nu}_j \psi_j$. Then, one can obtain

$$\bar{\nu}_j = \nu_j \beta_h(\tilde{\lambda}_j) + (1 - \beta_h(\tilde{\lambda}_j)), \quad (66)$$

where

$$\beta_h(\lambda) = \frac{2\Delta t}{T} \sum_{n=0}^M \eta_n \cos(\lambda t^n) \left(\cos(\omega t^n) - \frac{1}{4} \right). \quad (67)$$

Lemma 2.5 of [1] shows that $|\beta_h(\tilde{\lambda}_j)| \leq \rho_h := \max(1 - 0.3\delta^2, 0.63)$. Utilizing the fact that the composite trapezoidal rule is exact for pure periodic trigonometric functions of order less than the number of grid points, we complete the proof. \square

APPENDIX D

VERIFICATION OF TIME ERROR ELIMINATION IN YEE-EM-WAVEHOLTZ

With the modification in (34), $\tilde{\omega}$ in Theorem 1 becomes

$$\frac{\sin(\tilde{\omega}\Delta t/2)}{\Delta t/2} = \omega.$$

Meanwhile, (64) becomes

$$(\tilde{E}_z)_j^n = (\nu_j - \nu_j^\infty) \cos(\tilde{\lambda}_j t^n) + \nu_j^\infty \cos(\tilde{\omega} t^n), \quad (68)$$

and the original composite trapezoidal quadrature is no longer exact for $\nu_j^\infty \cos(\tilde{\omega} t^n)$. Hence, the modification (35) to the numerical quadrature is needed to eliminate time error from the numerical integration.

REFERENCES

- [1] D. Appelö, F. Garcia, and O. Runborg, "WaveHoltz: iterative solution of the Helmholtz equation via the wave equation," *SIAM Journal on Scientific Computing*, vol. 42, no. 4, pp. A1950–A1983, 2020.
- [2] A. Taflové and S. Hagness, *Computational electrodynamics: the Finite-Difference Time-Domain method*, 3rd ed. Artech House, 2005.
- [3] J. Hesthaven and T. Warburton, "Nodal high-order methods on unstructured grids: I. time-domain solution of Maxwell's equations," *J. Comput. Phys.*, vol. 181, pp. 186–221, 2002.
- [4] M.-O. Bristeau, R. Glowinski, and J. Périaux, "Controllability methods for the computation of time-periodic solutions; application to scattering," *Journal of Computational Physics*, vol. 147, no. 2, pp. 265–292, 1998.
- [5] M. J. Grote and J. H. Tang, "On controllability methods for the Helmholtz equation," *Journal of Computational and Applied Mathematics*, vol. 358, pp. 306–326, 2019.
- [6] M.-O. Bristeau, R. Glowinski, J. Périaux, and T. Rossi, "3D harmonic Maxwell solutions on vector and parallel computers using controllability and finite element methods," Ph.D. dissertation, INRIA, 1999.
- [7] D. Pauly and T. Rossi, "Theoretical considerations on the computation of generalized time-periodic waves," *arXiv preprint arXiv:1105.4095*, 2011.
- [8] J. Rabinä, S. Mönkölä, T. Rossi, A. Penttilä, and K. Muinonen, "Comparison of discrete exterior calculus and discrete-dipole approximation for electromagnetic scattering," *Journal of Quantitative Spectroscopy and Radiative Transfer*, vol. 146, pp. 417–423, 2014.
- [9] W. C. Chew, J.-M. Jin, and E. Michielssen, *Fast and efficient algorithms in computational electromagnetics*. Artech house, 2001.
- [10] F. P. Andriulli, K. Cools, H. Bagci, F. Olyslager, A. Buffa, S. Christiansen, and E. Michielssen, "A multiplicative Calderon preconditioner for the electric field integral equation," *IEEE Transactions on Antennas and Propagation*, vol. 56, no. 8, pp. 2398–2412, 2008.
- [11] A. Toselli and O. Widlund, *Domain decomposition methods-algorithms and theory*. Springer Science & Business Media, 2006, vol. 34.
- [12] S.-C. Lee, M. N. Vouvakis, and J.-F. Lee, "A non-overlapping domain decomposition method with non-matching grids for modeling large finite antenna arrays," *Journal of Computational Physics*, vol. 203, no. 1, pp. 1–21, 2005.
- [13] M. N. Vouvakis, Z. Cendes, and J.-F. Lee, "A FEM domain decomposition method for photonic and electromagnetic band gap structures," *IEEE Transactions on Antennas and Propagation*, vol. 54, no. 2, pp. 721–733, 2006.
- [14] Z. Peng, V. Rawat, and J.-F. Lee, "One way domain decomposition method with second order transmission conditions for solving electromagnetic wave problems," *Journal of Computational Physics*, vol. 229, no. 4, pp. 1181–1197, 2010.
- [15] Z. Peng and J.-F. Lee, "Non-conformal domain decomposition method with second-order transmission conditions for time-harmonic electromagnetics," *Journal of Computational Physics*, vol. 229, no. 16, pp. 5615–5629, 2010.
- [16] V. Dolean, M. J. Gander, S. Lanteri, J.-F. Lee, and Z. Peng, "Effective transmission conditions for domain decomposition methods applied to the time-harmonic curl-curl Maxwell's equations," *Journal of computational physics*, vol. 280, pp. 232–247, 2015.
- [17] Z. Peng, X.-c. Wang, and J.-F. Lee, "Integral equation based domain decomposition method for solving electromagnetic wave scattering from non-penetrable objects," *IEEE Transactions on Antennas and Propagation*, vol. 59, no. 9, pp. 3328–3338, 2011.
- [18] M. Bonazzoli, V. Dolean, I. Graham, E. Spence, and P.-H. Tournier, "Domain decomposition preconditioning for the high-frequency time-harmonic Maxwell equations with absorption," *Mathematics of Computation*, vol. 88, no. 320, pp. 2559–2604, 2019.
- [19] R. Hiptmair, "Multigrid method for Maxwell's equations," *SIAM Journal on Numerical Analysis*, vol. 36, no. 1, pp. 204–225, 1998.
- [20] J. Gopalakrishnan, J. E. Pasciak, and L. F. Demkowicz, "Analysis of a multigrid algorithm for time harmonic Maxwell equations," *SIAM Journal on Numerical Analysis*, vol. 42, no. 1, pp. 90–108, 2004.
- [21] P. Lu and X. Xu, "A robust multilevel method for the time-harmonic Maxwell equation with high wave number," *SIAM Journal on Scientific Computing*, vol. 38, no. 2, pp. A856–A874, 2016.
- [22] P. Tsuji and L. Ying, "A sweeping preconditioner for Yee's finite difference approximation of time-harmonic Maxwell's equations," *Frontiers of Mathematics in China*, vol. 7, no. 2, pp. 347–363, 2012.
- [23] P. Tsuji, B. Engquist, and L. Ying, "A sweeping preconditioner for time-harmonic Maxwell's equations with finite elements," *Journal of Computational Physics*, vol. 231, no. 9, pp. 3770–3783, 2012.
- [24] C. Morawetz, "The limiting amplitude principle," *Communications on Pure and Applied Mathematics*, vol. 15, no. 3, pp. 349–361, 1962.
- [25] K. Yee, "Numerical solution of initial boundary value problems involving Maxwell's equations in isotropic media," *IEEE Transactions on antennas and propagation*, vol. 14, no. 3, pp. 302–307, 1966.
- [26] A. Taflové and S. C. Hagness, *Computational electrodynamics: the finite-difference time-domain method*. Artech house, 2005.
- [27] J. S. Hesthaven and T. Warburton, *Nodal discontinuous Galerkin methods: algorithms, analysis, and applications*. Springer Science & Business Media, 2007.
- [28] B. Cockburn, G. E. Karniadakis, and C.-W. Shu, *Discontinuous Galerkin methods: theory, computation and applications*. Springer Science & Business Media, 2012, vol. 11.
- [29] J. W. Banks, B. B. Buckner, W. D. Henshaw, M. J. Jenkinson, A. V. Kildishev, G. Kovačič, L. J. Prokopeva, and D. W. Schwendeman, "A high-order accurate scheme for Maxwell's equations with a generalized dispersive material (GDM) model and material interfaces," *Journal of Computational Physics*, vol. 412, p. 109424, 2020.
- [30] F. Garcia, *Numerical methods for wave phenomena*. University of Colorado Boulder, 2021.
- [31] A. F. Oskooi, D. Roundy, M. Ibanescu, P. Bermel, J. D. Joannopoulos, and S. G. Johnson, "Meep: A flexible free-software package for electromagnetic simulations by the fdtd method," *Computer Physics Communications*, vol. 181, no. 3, pp. 687–702, 2010.
- [32] J. Lagrone, T. Hagstrom, and R. Chen, "rbcpack," <http://www.rbcpack.org>.
- [33] G. L. Sleijpen and D. R. Fokkema, "BiCGstab(l) for linear equations involving unsymmetric matrices with complex spectrum," *Electronic Transactions on Numerical Analysis*, vol. 1, pp. 11–32, 1993.
- [34] "Meep," <https://meep.readthedocs.io/>.
- [35] T. A. Davis and Y. Hu, "The University of Florida sparse matrix collection," *ACM Transactions on Mathematical Software (TOMS)*, vol. 38, no. 1, pp. 1–25, 2011.
- [36] P. G. Petropoulos, "Reflectionless sponge layers as absorbing boundary conditions for the numerical solution of maxwell equations in rectangular, cylindrical, and spherical coordinates," *SIAM Journal on Applied Mathematics*, vol. 60, no. 3, pp. 1037–1058, 2000.
- [37] J. LaGrone and T. Hagstrom, "Double absorbing boundaries for finite-difference time-domain electromagnetics," *Journal of Computational Physics*, vol. 326, pp. 650–665, 2016.
- [38] F. Assous, P. Ciarlet, and S. Labrunie, *Mathematical Foundations of Computational Electromagnetism*, ser. Applied Mathematical Sciences. Springer International Publishing, 2018.

Daniel Appelö Bio: Daniel Appelö holds a Ms degree in Electrical Engineering and a Ph. D. degree in Numerical Analysis from the Royal Institute of Technology in Sweden and is currently an Associate Professor in the Department of Computational Mathematics, Science and Engineering and the Department of Mathematics at Michigan State University.

Zhichao Peng Bio: Zhichao Peng holds a Ph. D. degree in Mathematics from the Rensselaer Polytechnic Institute in Troy, NY, USA in 2020. He is currently a research associate in the Department of Mathematics at Michigan State University.